Monthly Notices
of the
ROYAL ASTRONOMICAL SOCIETY

MNRAS **483,** 352–358 (2019)
Advance Access publication 2018 November 26

doi:10.1093/mnras/sty3186

RCW 120: a possible case of hit and run, elucidated by multitemperature dust mapping

K. A. Marsh [1,2]★ and A. P. Whitworth[1]

[1]*School of Physics and Astronomy, Cardiff University, Cardiff CF24 3AA, Wales, UK*
[2]*Infrared Processing and Analysis Center, California Institute of Technology, Pasadena, CA 91125, USA*

Accepted 2018 November 19. Received 2018 November 14; in original form 2018 September 24

ABSTRACT

We present resolution-enhanced images of warm dust at multiple temperatures and opacity index values in the star-forming bubble/H II region, RCW 120. The image set, representing a four-dimensional hypercube of differential column density, was obtained using our Bayesian procedure, PPMAP. The cool peripheral material (∼16–22 K) exhibits ragged clumpy structure as noted previously by others. However, at higher temperatures ($\lesssim$26 K) the geometry changes dramatically, showing a bubble boundary which is accurately circular in projection, except for the previously reported opening in the north. Comparison with *Spitzer* 8 μm data suggests that the ∼26–30 K dust seen by *Herschel* resides in the photodissociation region (PDR) surrounding the H II region. Its projected radial profile is consistent with that of a spherical shell, thus arguing against previous suggestions of cylindrical or planar geometry. The inferred geometry is, in fact, consistent with previous interpretations of the H II region as a classical Strömgren sphere, except for the fact that the ionizing star (CD −38° 11636; O8V) is displaced by more than half a radius from its geometric centre. None of the previously published models has satisfactorily accounted for that displacement. It could, however, be explained by proper motion of the O star at ∼2–4 km s^{-1} since its formation, possibly due to a cloud–cloud collision. We suggest that the current spherical bubble constitutes the fossilized remnant of the initial expansion of the H II region following the formation of the star, which now continues to flee its formation site.

Key words: stars: early-type – stars: formation – ISM: bubbles – dust, extinction – ISM: individual objects (RCW 120) – H II regions.

1 INTRODUCTION

RCW 120 is a Galactic H II region enclosed by a bubble of gas and dust which appears as a highly symmetrical shell in *Herschel* images. This shell is thought to be the site of triggered star formation by the collect and collapse process (Zavagno et al. 2007) or radiatively driven implosion of pre-existing condensations (Walch et al. 2015). The origin of the shell, however, is not clear. Two possibilities that have been proposed are:

(i) The *expanding* H II*region* model. In this interpretation, an O star forms within an approximately uniform interstellar medium (ISM), giving rise to a surrounding Strömgren sphere of ionized gas. The expansion of this gas results in a shock front which travels outwards, initially at the sound speed, sweeping out a dense shell of molecular gas (Zavagno et al. 2007; Deharveng et al. 2009). A variant of this model involves an O star in a Bonnor–Ebert sphere rather than a uniform ISM, whereby the O star location is postulated to be far off-centre (Ochsendorf et al. 2014).

(ii) The *cloud–cloud collision* model. Star formation by cloud–cloud collisions was investigated by Habe & Ohta (1992) and proposed as an explanation for the formation of RCW 120 by Torii et al. (2015). Their model involves a collision velocity of ∼30 km s^{-1}, as suggested by the observed radial velocities of −8 km s^{-1} for the ring, and −28 km s^{-1} for an adjacent cloud which appears to be physically connected.

In this paper we present the results of our investigation of the dust distribution in RCW 120 using *Herschel* data in conjunction with a new Bayesian analysis procedure, PPMAP (Marsh, Whitworth & Lomax 2015) that yields significantly higher spatial resolution than conventional techniques and provides information on the distribution of dust temperatures and dust opacity index values along the line of sight.

2 METHODOLOGY

In contrast with previous approaches to the dust mapping problem, the PPMAP procedure drops the assumptions of uniform dust

★ E-mail: ken.marsh@astro.cf.ac.uk

temperature and opacity index along the line of sight (Marsh et al. 2015).[1] After taking proper account of the point spread function and spectral response of the telescope, it returns a four-dimensional hypercube of estimated differential column density as a function of sky location (RA, Dec.), dust temperature, T_D and opacity index, β, assuming a power-law variation of opacity with wavelength. It also returns a corresponding hypercube of uncertainty values.

The procedure assumes only that the the emission is optically thin over the range of observed wavelengths. It works by defining a grid of discrete values of x, y, T_D, and β, which represent sampling locations in the continuous state space of (x, y, T_D, β). It then iterates towards the set of differential column densities, in the vicinities of those grid points, that best reproduces the observed monochromatic intensities. The resolution on the plane of the sky (x, y) is increased by a factor of about 4.5 relative to the standard analysis procedure, yielding maps of RCW 120 with an angular resolution of ∼8 arcsec, sampled by 4 arcsec square pixels.

The dust temperature sampling interval is arbitrary. For this work, we have used 12 representative dust temperatures, logarithmically spaced between 8 and 50 K. The opacity index sampling interval is also arbitrary, and we have used five representative values equally spaced linearly between 1.5 and 2.5. Our column density scale is based on an assumed opacity of 0.1 cm^2 g^{-1} at a wavelength of 300 μm. This reference opacity is defined with respect to total mass (dust plus gas). Although observationally determined, it is consistent with a gas to dust ratio of 100 (Hildebrand 1983).

3 OBSERVATIONS

RCW 120 was observed as part of the Hi-GAL survey (Molinari et al. 2010) using the *Herschel* PACS and SPIRE instruments which provided continuum images in bands centred on wavelengths of 70, 160, 250, 350, and 500 μm. The spatial resolution values of these data, i.e. the beam sizes at full width half-maximum, are approximately 8.5, 13.5, 18.2, 24.9, and 36.3 arcsec, respectively. The details of the calibration and map-making procedures are given by Elia et al. (2013). For our analysis we use PSFs based on the measured *Herschel* beam profiles (Poglitsch et al. 2010; Griffin et al. 2013).

4 RESULTS

The above data have been used to generate a four-dimensional hypercube of differential column density as a function of sky location, dust temperature, and dust opacity index, from which we can derive various line-of-sight integrated quantities such as the integrated column density of dust plus gas, N, the mean dust temperature, $\bar{T}$, and the mean dust opacity index $\bar{\beta}$.

Fig. 1 shows a set of images of differential column density for all 12 temperatures, each image having been summed over opacity index. The corresponding uncertainties are presented in Fig. 2.

Fig. 3 shows the line-of-sight integrated quantities derived from the differential column density hypercube, namely the total column density and density-weighted mean values of dust temperature and opacity index.

Comparison of the lower two panels in Fig. 3 suggests that localized minima in dust temperature (presumably cores) correspond

[1]The original version treated the opacity index, β, as constant. We have extended the algorithm by treating β as an additional state variable, as discussed in detail by Marsh et al. (2018).

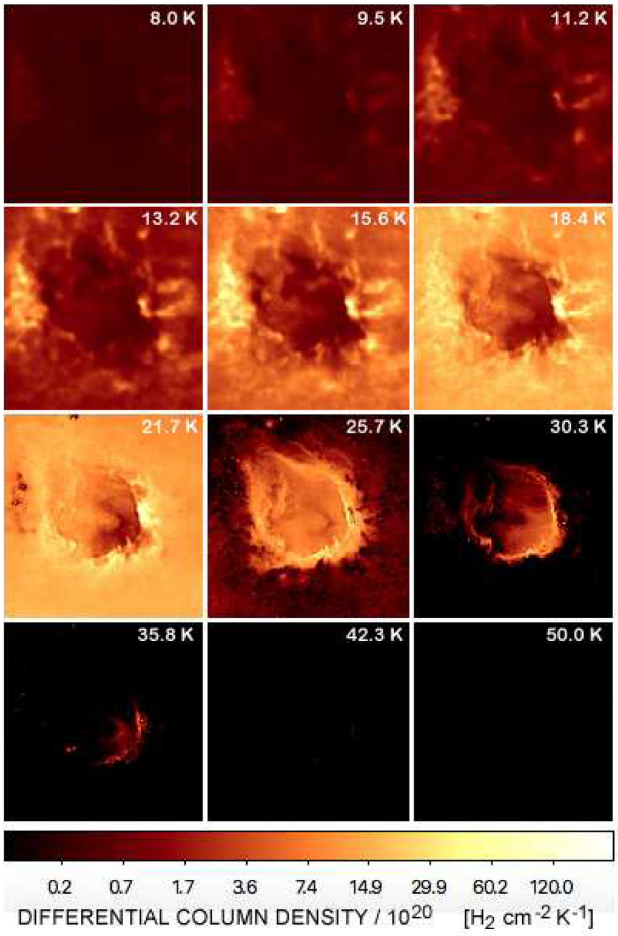

Figure 1. Maps of differential column density as a function of temperature. The field of view in each case is 21 arcmin (8.2 pc) square.

to local minima in dust opacity index, β. This behaviour is quite apparent in the scatter plot of β versus T shown in Fig. 4, which does not show the anticorrelation found by Anderson et al. (2010). But as pointed out by those authors, their anticorrelation may reflect the well-known β-T degeneracy in the presence of noise (Shetty et al. 2009). Given that the dust is optically thin at all of the *Herschel* wavelengths, the occurrence in cool dense clumps, of β values smaller than those in the surrounding ISM, is suggestive of grain growth (Rodmann et al. 2006).

An alternative way of representing the variation of differential column density with temperature, besides the multipanel format of Fig. 1, is to use composite overlays in which different temperatures are represented by different colours. The upper two panels of Fig. 5 present such multitemperature composites. In order to cover the entire 8–50 K range involved in the PPMAP output, however, it was necessary to split the temperatures into two separate temperature ranges, namely (a) cool (8–22 K) and (b) warm (26–50 K).

It is evident that the geometry of RCW 120 is dramatically different when viewed in the two temperature ranges. At the cooler temperatures ($\gtrsim$ 22 K), a ragged geometry is evident, corresponding to the presence massive clumps around the periphery, consistent with the findings of previous authors (Zavagno et al. 2007; Deharveng et al. 2009). However, at the higher temperatures ($\lesssim$26 K) the geometry changes dramatically, showing a bubble boundary which appears accurately circular in projection, except for the previously reported opening in the north (Zavagno et al. 2007). A comparison

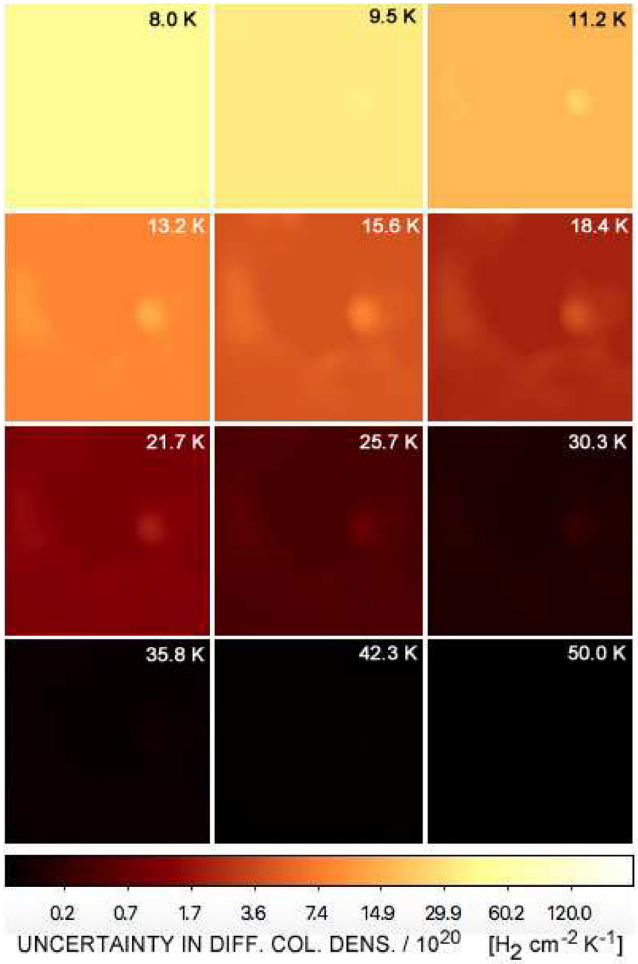

Figure 2. Uncertainties in the differential column density maps in Fig. 1 as a function of temperature.

between the bottom two panels of Fig. 5 shows a detailed correspondence between the distribution of 26–30 K dust and that of 8 μm emission seen by *Spitzer*. This is quite remarkable given that the emission mechanisms are different in the two cases, representing thermal emission by dust grains in the former case, and the fluorescence of PAHs in the ultraviolet field of the ionizing star in the case of the 8 μm emission (Zavagno et al. 2007). The detailed morphological correspondence suggests that the ∼26–30 K dust seen by *Herschel* resides in the hot photodissociation region (PDR) surrounding the H II region.

The geometry of the rim of the bubble is indicated more clearly in Fig. 6 which shows the distribution of differential column density in a narrow temperature range centred on 30 K after subtracting a median-filtered background. For comparison, the best-fitting circle is shown in orange, with the geometric centre indicated by the ' + ' sign. Evidently, the projected edge of the bubble is accurately circular over a wide angular range (∼315°), and this places constraints on formation models, as discussed below.

The question arises as to whether the circular outline represents a sphere seen in projection. This question is relevant since the three-dimensional geometry of such objects such as RCW 120 is still unclear (Anderson et al. 2015). For example, Deharveng et al. (2009) ask whether the geometry might involve a preferred plane, while Pavlyuchenkov, Kirsanova & Wiebe (2011) suggest that the H II region of RCW 120 is cylindrical rather than spherical and that

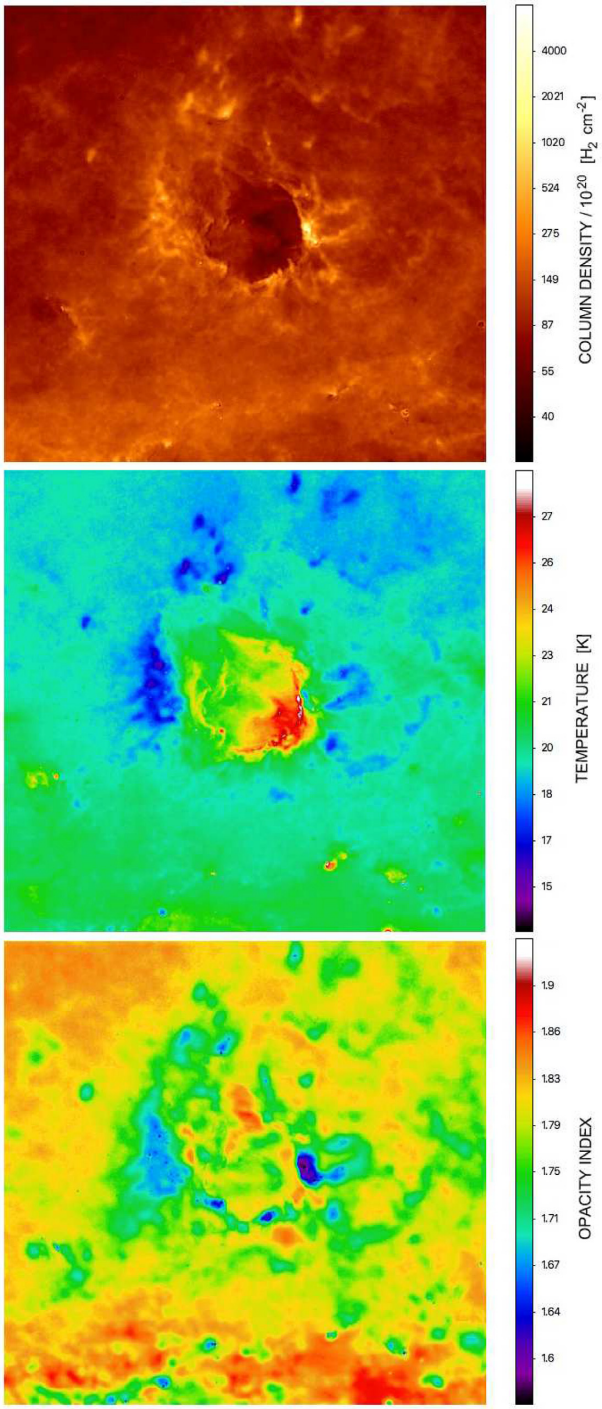

Figure 3. Maps of line-of-sight integrated quantities, namely *Top:* total column density, *Middle:* density-weighted mean dust temperature, and *Bottom:* density-weighted mean dust opacity index. The field of view in each case is 42 × 42 arcmin.

we are observing the object along the axis of the cylinder. A similar suggestion has been made by Torii et al. (2015) in connection with their cloud–cloud collision model. We can use the PPMAP results to investigate this question, based on the assumption that the 26–30 K dust maps the PDR as suggested above. Specifically we can check to see if the edge-to-centre contrast of the differential column density is consistent with that expected for a hollow shell whose wall has

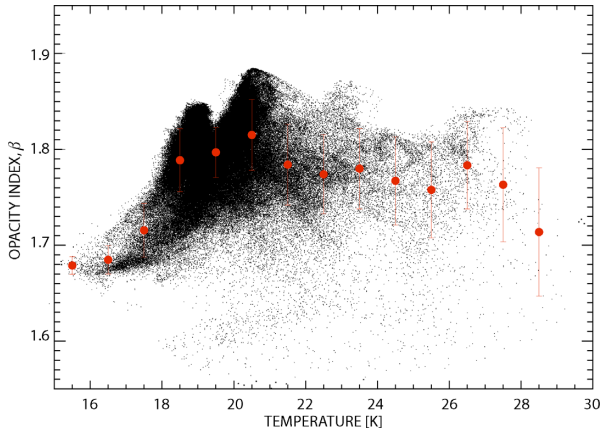

Figure 4. Scatter plot of dust opacity index versus temperature. Each black plotted point represents one pixel from Fig. 3. The red filled circles and corepsonding error bars represent 2σ trimmed means and standard deviations.

a finite thickness. To facilitate this check, Fig. 7 shows the radial profile of differential column density, azimuthally averaged about the centre, indicated by the ' + ' sign in Fig. 6. The abcissa of this plot represents the projected distance, h, from the geometric centre. We can compare this plot with the expected profile, $N_{\rm mod}(h)$, of an optically thin, uniform hollow shell with inner and outer radii $r_{\rm in}$ and $r_{\rm out}$, respectively, i.e.

$$N_{\rm mod}(h) = \begin{cases} 2n_0(\sqrt{r_{\rm out}^2 - h^2} - \sqrt{r_{\rm in}^2 - h^2}) & \text{if } h \le r_{\rm in}, \\ 2n_0\sqrt{r_{\rm out}^2 - h^2} & \text{if } r_{\rm in} < h < r_{\rm out}, \\ 0 & \text{otherwise,} \end{cases} \quad (1)$$

where n_0 is the volume density, given by $n_0 = N_0/(r_{\rm out} - r_{\rm in})$, and N_0 represents the column density through the shell wall at the projected centre.

We constrain the parameters N_0, $r_{\rm in}$, and $r_{\rm out}$ using estimates derived from the observed profile ($N_0 = 12.25 \pm 0.07 \times 10^{20}$ H_2 cm $^{-2}$, $r_{\rm in} = 1.66$ pc, $r_{\rm out} = 1.98$ pc) and thereby obtain the model profile shown as a dotted line in Fig. 7. It reproduces well the behaviour of the observed profile except for the existence of a tail beyond the peak, which we interpret as the halo of filamentary material attributed to leakage from the bubble (Zavagno et al. 2007) and which is evident in the middle panel of Fig. 5. In particular, the simple model reproduces the observed edge-to-centre contrast. The theoretical value for the model sphere is 3.37, which compares well with the observed value of 3.15 ± 0.18. This provides support for the interpretation of spherical geometry for the bubble.

It does, however, contrast sharply with the findings of Pavlyuchenkov et al. (2011) who concluded that a spherical shell does not fit the observed profile of *Herschel* 100 μm emission. However, the latter is not a reliable proxy for column density because a temperature gradient is present, such that the dust temperature decreases outwards from the hot (∼30 K) inner rim. Consequently, the 100 μm emission is biased towards the rim even though there is cooler dust (∼26 K) further out in the PDR, as evidenced by its correspondence with 8 μm emission as shown in Fig. 5. Thus the PDR shell is thicker than suggested by the 100 μm emission and, as a consequence, has significant column density through the projected centre of the ring (see Fig. 7). That feature represents a key difference from the profile upon which the conclusions of Pavlyuchenkov et al. (2011) were based.

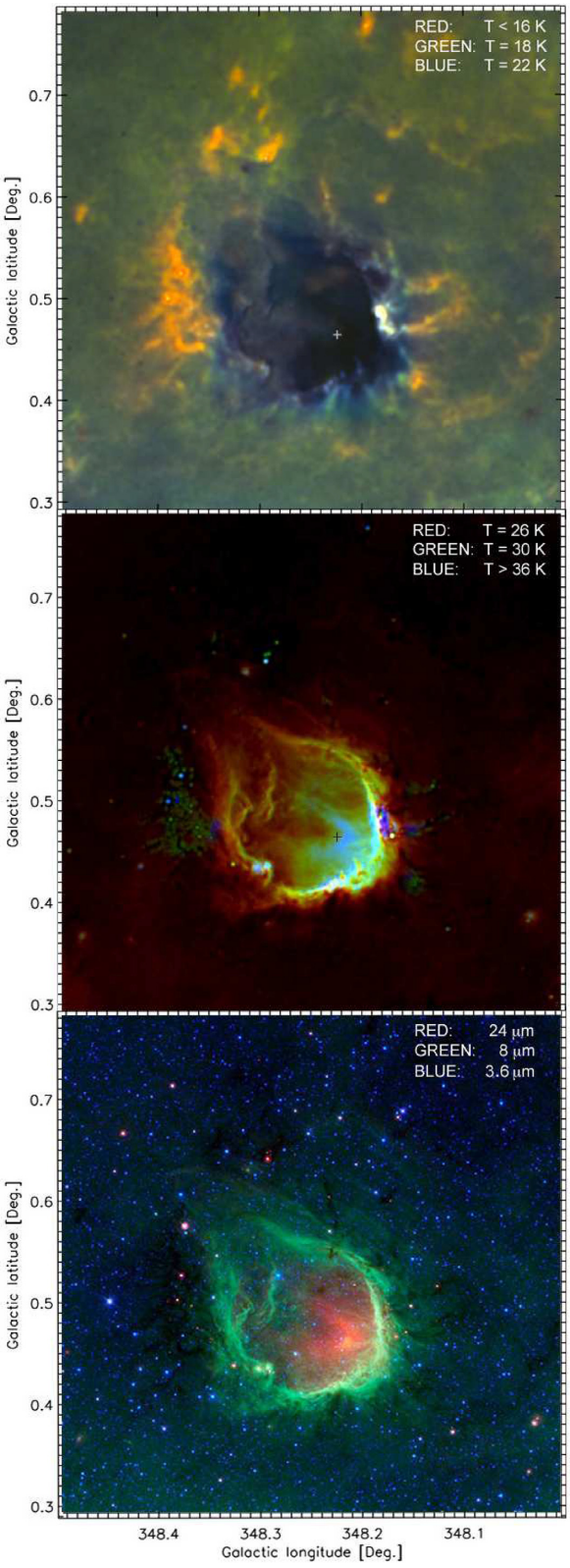

Figure 5. Composite images of RCW 120. The top two panels represent multitemperature overlays, with red, green, and blue corresponding to the indicated temperature ranges. The ' + ' signs mark the O star position. For comparison, the bottom panel shows a multiwavelength composite from *Spitzer*. Note the detailed correspondence between the 8 μm IRAC image (shown in green) with the 26–30 K dust (shown red and green in the middle panel).

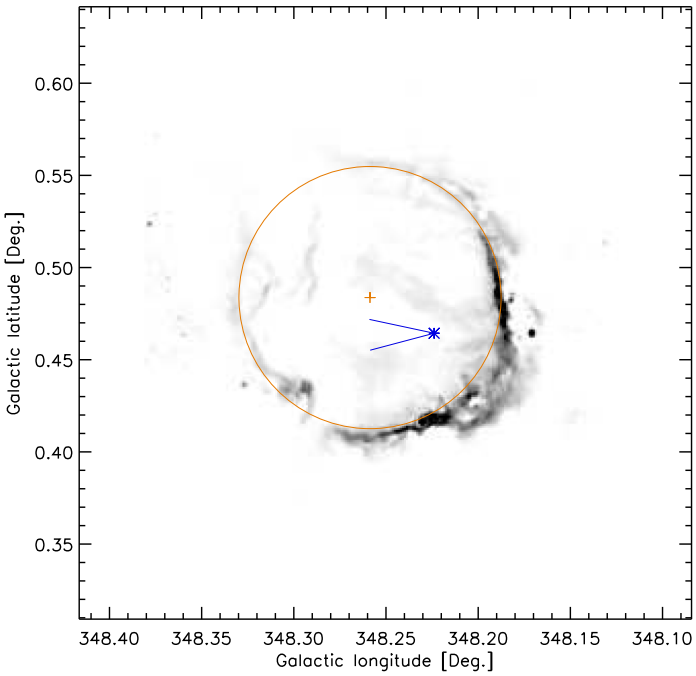

Figure 6. The greyscale image represents the bright rim of the 30 K dust distribution in RCW 120 which presumably delineates the edge of the PDR, as discussed in the text. The best-fitting circle is indicated in orange; its geometric centre is indicated by the ' + ' sign. The blue asterisk represents the current position of the ionizing star. The blue lines represent the 1σ limits of previous proper motion of the O star over the past 3.2×10^4 yr based on *Gaia* observations. Note, however, that during this time the ring structure itself would have moved also.

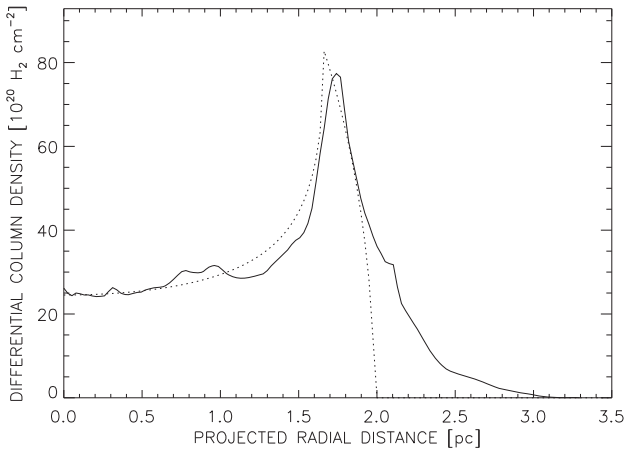

Figure 7. The radial distribution of warm dust in the PDR. The solid line represents the azimuthally averaged distribution of differential column density in the temperature range 26–30 K, as estimated using PPMAP. It is expressed as a function of the projected distance from the centre of symmetry as indicated in Fig. 6. The dotted line represents the theoretical profile based on a three-parameter model of a hollow sphere whose inner radius, outer radius, and central column density are derived from the observations.

5 DISCUSSION

The above results strongly suggest that the RCW 120 bubble is spherical except for an opening in the north, attributed to a 'champagne flow' of ionized gas leaking out of the bubble (Zavagno et al. 2007). One particularly puzzling aspect, however, is that the ionizing star, CD−38°.11636 (Zavagno et al. 2007), is displaced far from the geometric centre of the sphere, as shown in Fig. 6.

The observed geometry is, in fact, inconsistent with all of the formation models proposed in the literature so far. In particular, the classical 'expanding H II region' model would place the ionizing star at the centre of the bubble, in contrast to the observed geometry illustrated in Fig. 6. Although Zavagno et al. (2007) explain the displacement as due to a north–south density gradient, the ionization front would then be egg-shaped rather than spherical. While the displacement could, in principle, be explained if the star were postulated to be located off-centre in a Bonnor–Ebert sphere (Ochsendorf et al. 2014), such a model leads to an irregularly shaped ionization zone, contrary to observation. In addition, it fails to reproduce the observed distribution of CO (Torii et al. 2015).

In the case of the cloud–cloud collision model as interpreted by Torii et al. (2015), the bubble boundary would correspond to the inner edge of a U-shaped cavity rather than a near-perfect ring which, again, is contrary to observation. Although the authors do point out that a ring-like appearance could result from a viewing angle along the axis of cylindrical symmetry in their model, the star would then appear near the centre of the ring in projection and would not show the observed displacement.

One piece of information that has not been exploited in previous analyses, however, is that the O star has a large proper motion. The *Gaia* DR2 catalogue (Gaia Collaboration: Brown et al. 2018) indicates motion in RA and Dec. of -3.05 ± 0.89 mas yr^{-1} and -3.12 ± 0.63 mas yr^{-1}, corresponding to a net transverse motion of 28 ± 5 km s^{-1}, mostly in the direction of decreasing Galactic longitude, i.e. away from the geometric centre of the ring. It is therefore of interest to ask where the O star would have been at the time of formation of the H II region. In the absence of proper motion of the ring itself, a backward extrapolation of the O star proper motion would have placed the latter within the wedge-shaped 1σ limits delineated in blue in Fig. 6. Closest approach would have

occurred $\sim 3.2 \times 10^4$ yr ago, with the O star missing the geometric centre by approximately 2.4σ.

However, the molecular ring undoubtedly has some proper motion of its own, and this would need to be taken into account in order to determine the previous trajectory of the O star relative to the ring. Unfortunately there are currently no observational data that would permit such a determination. For example, even though several compact sources are present in the molecular ring (Figueira et al. 2017), none has a convincing match with a *Gaia* object. Conversely, although matches exist between *Gaia* objects and published positions of YSOs (Zavagno et al. 2007; Martins et al. 2010), none has a convincing association with structure in the molecular ring. So the only available information on the transverse proper motion of the ring is the mean Galactic rotation in the vicinity, namely -0.84 mas yr^{-1} in longitude (equivalent to -5.4 km s^{-1}), based on the most recent Galactic rotation curve (Russeil et al. 2017). The corresponding radial velocity would be -8.5 km s^{-1}, consistent with the observed -8 km s^{-1} radial velocity of the molecular ring[2] (Anderson et al. 2015; Torii et al. 2015; Sánchez-Cruces et al. 2018)

So in summary, in the absence of any measurements of proper motion of the molecular ring, we cannot establish the previous trajectory of the O star with respect to it. However, if we make the assumption that the O star was, at some previous time, located in the centre of the ring, then its current displacement can be understood as a natural consequence of proper motion since that time. We now explore the implications of that assumption, starting with the epoch of formation of the O star, whose mass is assumed to be $\sim 20\,M_\odot$. For simplicity we assume that its ionizing radiation is isotropic and that the ambient ISM is approximately uniform.

The O star would have evolved rapidly, with the photospheric temperature increasing on a time-scale $\sim 10^4$ yr on the approach to the main sequence (Hosokawa & Omukai 2009; Davies et al. 2011). It would then have ionized the surrounding gas on an even shorter time-scale ($\sim$40 yr), at which point the resulting spherical H II region would have expanded and swept up a dense surrounding shell in a fashion similar to that envisaged by Zavagno et al. (2007) and Deharveng et al. (2009). The key difference is that, following the formation of the shell, the O star would have continued to move through the cloud. The shell would continue to expand, but the dust contained within it would form a barrier to the ionizing photons, thus maintaining a spherical boundary to the H II region. The observed bubble would then represent the fossilized remnant of the initial expansion of the H II region.

The time, t, taken for the H II region to expand from the radius, $R_{\rm si}$, of the initial Strömgren sphere to its current radius, R (1.7 pc), can be obtained from the analytical expressions given by Spitzer (1978), which yield

$$t = \frac{4}{7}\frac{R_{\rm si}}{c_{\rm s}}\left[\left(\frac{R}{R_{\rm si}}\right)^{\frac{7}{4}} - 1\right], \qquad (2)$$

where $c_{\rm s}$ is the sound speed in ionized hydrogen and $R_{\rm si}$ is given by

$$R_{\rm si} = \left[\frac{3}{4\pi}\frac{\mathcal{L}}{n_{\rm i}^2 \alpha_{\rm B}}\right]^{\frac{1}{3}}. \qquad (3)$$

[2]These two radial velocities would not be independent if we simply used the kinematic distance (1.35 kpc), but there exists an independent photometric estimate of 1.33 kpc (Zavagno et al. 2007).

Here $n_{\rm i}$ is the number density of neutral hydrogen atoms in the ambient cloud, $\mathcal{L}$ is the ionizing photon luminosity, and $\alpha_{\rm B}$ is the case-B recombination coefficient for ionized hydrogen at 10^4 K, which we take as 2.7×10^{-13} cm^3 s^{-1} (Bisbas et al. 2015). Further, assuming $n_{\rm i}$ to be in the range 1000–3000 cm^{-3} and $\mathcal{L} = 10^{48.04}$ photons s^{-1} (Zavagno et al. 2007; Arthur et al. 2011) together with a sound speed, $c_{\rm s} = 13$ km s^{-1}, appropriate to ionized hydrogen at 10^4 K, we obtain a range of expansion times of 0.23–0.42 Myr, consistent with previous estimates (Zavagno et al. 2007; Anderson et al. 2015; Mackey et al. 2015).

During this interval, the O star will have moved a projected distance Δr from the location of ionization onset to its current location. Based on the geometry illustrated in Fig. 6, we estimate this distance to be 0.93 pc. The component of O star velocity with respect to the shell in a plane transverse to the line of sight is then $v_{\rm T} = \Delta r/t$, giving a range of possible values 2.2–3.9 km s^{-1}. The motion would be at a position angle of approximately 241° with respect to Galactic north. Doing a vector subtraction of these velocities from the observed proper motion of the O star (from *Gaia*) gives the implied proper motion of the molecular ring, whose components in the longitude and latitude directions would then be ~ -25 km s^{-1} and ~ 5 km s^{-1}, respectively.

We note that our explanation for the spherical shell, in terms of a fossilized remnant of initial H II region expansion, is not consistent with the results of the simulation by Mackey et al. (2015) which predict an egg-shaped boundary for the H II region. Those simulations were nevertheless based on reasonable parameters for RCW 120, which included an O star moving with velocity 4 km s^{-1} through a uniform ISM of hydrogen number density 3000 cm^{-3}, taking account of the effects of a stellar wind bubble. They predict that after an elapsed time of 0.4 Myr, the ratio of major to minor axes of the ionization boundary would be approximately 1.4. This, however, is inconsistent with the observational result shown in Fig. 6 which indicates no more than ±5 per cent deviation from circularity. A possible explanation for the discrepancy is the neglect of dust in the Mackey et al. (2015) simulations, since dust may have a significant effect on the shape of the ionized region. The importance of dust is suggested by the fact that more than 50 per cent of all of the ionizing photons are absorbed by dust within the H II region in the initial stages of evolution (Arthur et al. 2011). In the context of the evolutionary scenario outlined above, the dust might be expected to prevent ionizing photons from travelling beyond the boundaries of the expanding shell (whose geometry is established early on), thus preventing the ionized region from morphing into an egg shape. Confirmation, however, will need to await numerical simulation.

If the above model is correct, then the O star will have been born in relative motion with its parent cloud, the transverse component of its relative velocity being $\sim$2–4 km s^{-1}. The question then arises as to the origin of this motion. Possibilities are:

(i) The O star resulted from a cloud–cloud collision (Habe & Ohta 1992; Torii et al. 2015).

(ii) The O star was born in a single cloud, acquiring its space velocity from supersonic turbulence. Mackey et al. (2015) have postulated that space velocities $\sim$2–5 km s^{-1} can arise from such a mechanism, but no quantitative predictions appear to be available, based either on simulations or theory. It is therefore unclear whether it can account for stellar motion in RCW 120.

(iii) Dynamical ejection from a binary or higher order multiple system (Renzo et al. 2018). Such a mechanism could, in principle, provide a massive star with a space velocity of a few km s^{-1} with

respect to its parent cloud, but it is probably not viable in the case of RCW 120 since the O star has no nearby companions of comparable mass.

So based on currently available information, the cloud–cloud collision model (Torii et al. 2015) seems to provide the most viable scenario. The formation of the O star is then attributed to the collision of two clouds with an impact velocity of 20 km s^{-1} in the radial direction. This model predicts that the O star would continue moving through the H II region with somewhat less than the original impact speed.

An interesting feature of the dust maps in Fig. 5 is an arc-shaped region which appears in blue in the middle panel, representing the warmest dust detected by *Herschel* (>36 K), and in red in the corresponding *Spitzer* image, representing 24 μm emission. Although its spatial relationship with the O star is reminiscent of a bow shock, such an interpretation is unlikely given the star's probable subsonic motion. We base the latter on a ∼7 km s^{-1} upper limit for the star's speed relative to the shell, dictated by the requirement that the star still be located within the boundary of the shell, given the inferred lower limit (0.23 Myr) of the expansion time-scale. More viable interpretations of the arc-shaped feature include the effects of stellar winds from subsonically moving stars (Mackey et al. 2015) and 'dust waves' due to the dragging effect of radiation pressure on flowing gas (Ochsendorf et al. 2014).

Finally, we note that if the cloud–cloud collision model is applicable to RCW 120, the O star would presumably be the largest member of a whole cluster of stars produced during the collision, since recent simulations (Balfour et al. 2015; Balfour, Whitworth & Hubber 2017) have shown that such an event can result in a distribution of protostars in a web-like or hub-and-spoke configuration. However, the latter simulations were based on a regime of parameter space very different from that in the Torii et al. (2015) model, in that they involved the collision of clouds of *similar* mass at *low* relative velocity (≤4 km s^{-1}). Because of the likelihood that cloud–cloud collisions account for a substantial fraction of massive star formation it will be important to expand the scope of future simulations and continue the analysis of observations of other objects similar to RCW 120.

In summary, we present evidence that the warm dust in the PDR associated with the H II region is distributed in a spherical shell. The displacement of the O star from the geometric centre can be explained by proper motion since the formation of the shell. The velocities involved are consistent with the cloud–cloud collision model as envisaged by Torii et al. (2015), but we interpret the bubble boundary as the fossilized remnant of a swept-up shell rather than as the interior of a U-shaped cavity.

ACKNOWLEDGEMENTS

We thank the referee for helpful comments. We also gratefully acknowledge the support of a consolidated grant (ST/K00926/1) from the UK Science and Technology Funding Council. This work was performed using the computational facilities of the Advanced Research Computing at Cardiff (ARCCA) Division, Cardiff University. It has used data from the European Space Agency (ESA) mission *Gaia* (https://www.cosmos.esa.int/gaia), processed by the *Gaia* Data Processing and Analysis Consortium (DPAC, (https://www.cosmos.esa.int/web/gaia/dpac/consortium). Funding for the DPAC has been provided by national institutions, in particular the institutions participating in the *Gaia* Multilateral Agreement. The work is based, in part, on observations made with the Spitzer Space Telescope, which is operated by the Jet Propulsion Laboratory, California Institute of Technology under a contract with National Aeronautics and Space Administration (NASA).

REFERENCES

Anderson L. D. et al., 2010, A&A, 518, L99
Anderson L. D. et al., 2015, ApJ, 800, 101
Arthur S. J., Henney W. J., Mellema G., de Colle F., Vázquez-Semadeni E., 2011, MNRAS, 414, 1747
Balfour S. K., Whitworth A. P., Hubber D. A., Jaffa S. E., 2015, MNRAS, 453, 2471
Balfour S. K., Whitworth A. P., Hubber D. A., 2017, MNRAS, 465, 3483
Bisbas T. G. et al., 2015, MNRAS, 453, 1324
Davies B., Hoare M. G., Lumsden S. L., Hosokawa T., Oudmaijer R. D., Urquhart J. S., Mottram J. C., Stead J., 2011, MNRAS, 416, 972
Deharveng L., Zavagno A., Schuller F., Caplan J., Pomarès M., De Breuck C., 2009, A&A, 496, 177
Elia D. et al., 2013, ApJ, 772, 45
Figueira M. et al., 2017, A&A, 600, A93
Griffin M. J. et al., 2013, MNRAS, 434, 992
Habe A., Ohta K., 1992, PASJ, 44, 203
Hildebrand R. H., 1983, Q. J. R. Astron. Soc., 24, 267
Hosokawa T., Omukai K., 2009, ApJ, 691, 823
Mackey J., Gvaramadze V. V., Mohamed S., Langer N., 2015, A&A, A10, 573
Marsh K. A., Whitworth A. P., Lomax O., 2015, MNRAS, 454, 4282
Marsh K. A., Whitworth A. P., Smith M. W. L., Lomax O., Eales S. A., 2018, MNRAS, 480, 3052
Martins F., Pomarès M., Deharveng L., Zavagno A., Bouret J. C., 2010, A&A, 510, A32
Molinari S. et al., 2010, PASP, 122, 314
Ochsendorf B. B., Verdolini S., Cox N. L. J., Berné O., Kaper L., Tielens A. G. G. M., 2014, A&A, 566, A75
Pavlyuchenkov Ya. N., Kirsanova M. S., Wiebe D. S., 2013, Astron. Rep., 57, 573
Poglitsch A. et al., 2010, A&A, 518, L2
Renzo M. et al., 2018, preprint (arXiv:1804.09164v1)
Rodmann J., HenningT., Chandler C. J., Mundy L. G., Wilner D. J., 2006, A&A, 446, 211
Russeil D., Zavagno A., Mège P., Poulin Y., Molinari S., Cambresy L., 2017, A&A, 601, L5
Sánchez-Cruces M., Castellanos-Ramírez A., Rosado M., RodríguezGonzález A., Reyes-Iturbide J., 2018, Rev. Mex. Astron. Astrofis., 54, 375
Shetty R., Kauffmann J., Schnee S., Goodman A. A., 2009, ApJ, 696, 676
Spitzer L., 1978, Physical Processes in the Interstellar Medium. Wiley, New York
Torii K. et al., 2015, ApJ, 806, 7
Walch S., Whitworth A. P., Bisbas T. G., Hubber D. A., Wünsch R., 2015, MNRAS, 452, 2794
Zavagno A., Pomarès M., Deharveng L., Hosokawa T., Russeil D., Caplan J., 2007, A&A, 472, 835

This paper has been typeset from a TEX/LATEX file prepared by the author.